

Exciton-related luminescence of ZnO and its optoelectronic applications

Xiaoxuan Wang(王潇璇), Junfeng Lu(卢俊峰), Wendong Lu(卢文栋), Chaoyang Huang(黄朝阳), Chunxiang Xu(徐春祥)

Citation: Chin. Phys. B. 35, 097702 (2026). DOI: 10.1088/1674-1056/ae6f94 | CSTR: 32038.14.CPB.ae6f94
http://cpb.iphy.ac.cn; http://iopscience.iop.org/cpb

What follows is a list of articles you may be interested in

Manipulating optical and electronic properties through interfacial ferroelectricity

Yulu Liu(刘钰璐), Gan Liu(刘敢), Xiaoxiang Xi(奚啸翔)
Chin. Phys. B. 34, 017701 (2025). DOI: 10.1088/1674-1056/ad9456 | CSTR: 32038.14.CPB.ad9456

Indium doping effect on properties of ZnO nanoparticles synthesized by sol-gel method

S Mourad, J El Ghoul, K Omri, K Khirouni
Chin. Phys. B. 28, 047701 (2019). DOI: 10.1088/1674-1056/28/4/047701

High uniformity and forming-free ZnO-based transparent RRAM with HfOx inserting layer

Shi-Jian Wu(吴仕剑), Fang Wang(王芳), Zhi-Chao Zhang(张志超), Yi Li(李毅), Ye-Mei Han(韩叶梅), Zheng-Chun Yang(杨正春), Jin-Shi Zhao(赵金石), Kai-Liang Zhang(张楷亮)
Chin. Phys. B. 27, 087701 (2018). DOI: 10.1088/1674-1056/27/8/087701

Effect of O-O bonds on p-type conductivity in Ag-doped ZnO twin grain boundaries

Jingjing Wu(吴静静), Xin Tang(唐鑫), Fei Long(龙飞), Biyu Tang(唐壁玉)
Chin. Phys. B. 27, 057701 (2018). DOI: 10.1088/1674-1056/27/5/057701

TOPICAL REVIEW — Exciton physics: Fundamentals, materials and devices

Exciton-related luminescence of ZnO and its optoelectronic applications

Xiaoxuan Wang(王潇璇)[1], Junfeng Lu(卢俊峰)[2], Wendong Lu(卢文栋)[1], Chaoyang Huang(黄朝阳)[1], and Chunxiang Xu(徐春祥)[1,†]

[1] *School of Electronic Science and Engineering, Southeast University, Nanjing* 211189, *China*
[2] *College of Physics, Nanjing University of Aeronautics and Astronautics, Nanjing* 211106, *China*

(Received 28 February 2026; revised manuscript received 7 May 2026; accepted manuscript online 19 May 2026)

Excitons, as core elementary excitations in semiconductors, encompass fundamental scientific issues of longstanding interest in condensed matter physics and optoelectronics, including their formation, classification, dynamic behaviors, and radiative recombination mechanisms. This review focuses on excitons of zinc oxide (ZnO), a prototypical wide-bandgap semiconductor, highlighting its large exciton binding energy of ∼ 60 meV, its distinctive luminescence spectral structure, and the intrinsic physical origins that enable stable excitonic emission at room temperature. In the ZnO system, its exceptionally high exciton binding energy stems from weak dielectric screening and strong Coulomb interaction, endowing it with irreplaceable advantages for room-temperature ultraviolet optoelectronic devices. Besides, the exciton lasing in different ZnO micro/nano structures is introduced, as well as the applications such as the laser sensing and the ultraviolet light emitting devices. Moreover, the interactions of ZnO excitons with excitons, photons, phonons, and plasmons are mentioned and discussed. This review summarizes the exciton-related luminescence properties of ZnO, a material with great potential for functional optoelectronic applications.

Keywords: ZnO, exciton, luminescence, interactions, applications

PACS: 77.55.hf, 42.50.Ct, 42.55.Px, 42.55.Sa, 42.62.Fi, 42.65.Re, 78.47.D–

DOI: 10.1088/1674-1056/ae6f94 **CSTR:** 32038.14.CPB.ae6f94

1. Introduction

The interaction between light and matter stands as an enduring theme in physics and materials science. At its core, excitons (quasiparticles related to this interaction) related research spans from fundamental quantum mechanics to modern optoelectronic device applications. In semiconductors, the exciton is an electrically neutral quasiparticle consisting of an electron and a hole bound by Coulomb attraction. It serves as a foundational framework for understanding optical absorption, light emission, energy transport, and nonlinear optical responses in materials.[1–3] Either following photon excitation or carrier injection, their presence significantly modifies the physical properties of materials in excited states.[4–6] In-depth investigation of exciton behavior not only reveals the nature of many-body interactions in solids but also serves as the physical foundation for advancing modern optoelectronic technologies such as light-emitting diodes (LEDs), lasers, quantum light sources, and photonic chips. With the development of materials science, particularly the emergence of low-dimensional materials and wide-bandgap semiconductors, exciton physics has exhibited unprecedented richness and tunability.[7–9]

As a typical wide-bandgap semiconductor, zinc oxide (ZnO) has attracted widespread attention in optoelectronics due to its distinctive properties, including a direct bandgap of ∼ 3.37 eV, diverse morphologies amenable to device engineering, and a high exciton binding energy of ∼ 60 meV. This value substantially exceeds the thermal energy at room temperature (∼ 26 meV) and the exciton binding energies of conventional semiconductors such as GaN (∼ 26 meV), ZnSe (∼ 20 meV), and ZnS (∼ 37 meV).[10–12] It enables ZnO excitons to effectively remain in a non-ionized state at room temperature, thereby providing a solid physical foundation for achieving efficient near-band-edge (NBE) ultraviolet radiative recombination and has superior excitonic properties for optoelectronic devices. Hence, ZnO is considered an ideal candidate material for the fabrication of ultraviolet light-emitting diodes (UV-LEDs), laser diodes (LDs), and high-color-purity displays, demonstrating irreplaceable application potential in fields such as biomedical sterilization, water purification, short-distance high-speed communication, and high-density information storage.[13–17] Recently, ZnO devices with films, micrometer columns, two-dimensional structures, etc. have all been extensively studied both on basic performance and methods for constructing advanced devices.[18–23]

Therefore, this review introduces the types of excitons in ZnO and the process of exciton-related luminescence properties, further discusses exciton lasing behavior in ZnO mi-

†Corresponding author. E-mail: xcxseu@seu.edu.cn

© 2026 Chinese Physical Society and IOP Publishing Ltd. All rights, including for text and data mining, AI training, and similar technologies, are reserved.

cro/nanostructures. Furthermore, we analyze and compare the interactions between excitons in ZnO and excitons, photons, phonons, as well as plasmons, especially the influence on the exciton luminescence process. Finally, the applications of ZnO exciton luminescence are presented, including research progress related to electroluminescent devices and lasing-based sensors.

2. Exciton

An exciton is a collective electronic excitation (neutral bosonic quasiparticle) in a solid, formed by a Coulomb-correlated electron–hole pair that can propagate through the crystal lattice while transporting energy without net charge transport. The radiative recombination of free excitons manifests as narrow-band fluorescence with a small Stokes shift, where the emission energy is slightly lower than the bandgap.[24–26] The emission energy of conventional excitons is red-shifted relative to the fundamental bandgap energy (E_g) by an amount equal to the exciton binding energy.[27,28]

In materials with low exciton binding energies (below the room-temperature thermal energy of ~ 26 meV), thermal fluctuations readily induce exciton dissociation into free charge carriers. Consequently, excitonic luminescence in such materials can only be observed at cryogenic temperatures.[29–32] In contrast, materials with high binding energies, such as ZnO (~ 60 meV), sustain stable excitonic emission at room temperature with narrow spectral linewidths. However, in materials with strong exciton–phonon coupling, such as halide perovskites, an unusual type of emission arises from self-trapped excitons (STEs), whose emission energy is much smaller than the bandgap. In this case, the emission will be highly red-shifted, and the electrons and holes will be more severely restricted.[33,34] Due to the strong interaction between excitons and lattice vibrations (phonons), the exciton will lose some energy, called self-trapping energy (E_{st}), and become an STE. At the same time, the energy of the ground state will rise because of lattice deformation, and the increased energy is called lattice deformation energy (E_d). Consequently, as shown in Fig. 1(a), the emission energy can be described by $E_{PL} = E_g - E_b - E_{st} - E_d$, which is the origin of the large Stokes shift in STE emission.[35] STEs usually occur in materials with soft lattices and strong electron–phonon coupling, emitting photons with broad spectra and large Stokes shifts. For ZnO materials, excitonic emission can be observed at normal temperature in samples with high crystal quality. And ZnO quantum dots (QDs) and nanocrystals can exhibit typical STE emission characteristics under normal pressure. Recently, researchers introduced deviatory stress to modulate the STE process in pyramidal ZnO nanocrystals. This approach results in a remarkable shift in emission energy, from yellow-green (2.34 eV) to deep-blue (2.88 eV).[36]

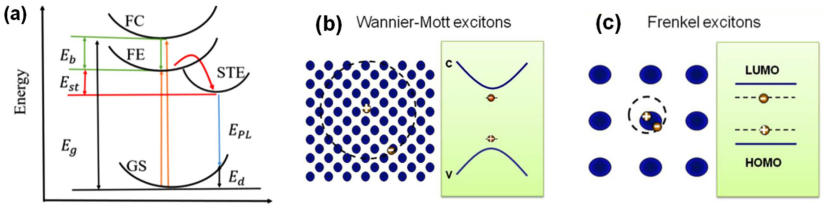


Fig. 1. (a) Schematic of the energy level structure of STE (GS, ground state; FE, free exciton state; FC, free carrier state; STE, self-trapped exciton state; E_g, bandgap energy; E_b, exciton binding energy; E_{st}, self-trapping energy; E_d, lattice deformation energy; E_{PL}, emission energy), which can be used to understand the origin of the large Stokes shift in STE emission.[35] (b), (c) Comparison between Wannier–Mott and Frenkel excitons.

Excitons are electrically neutral and therefore do not directly contribute to electrical conduction; however, their kinetic behavior profoundly influences the efficiency of photoelectric conversion. The physical characteristics of excitons are primarily described by two key parameters: binding energy and Bohr radius.[37,38] Among these, wide-bandgap semiconductors typically exhibit larger exciton binding energies and smaller Bohr radii due to their lower dielectric constants and weak Coulomb screening; conversely, narrow-bandgap materials possess smaller binding energies and more extended wavefunctions.[39,40]

The classification of excitons constitutes a multidimensional framework, primarily organized according to their confinement mechanisms, spatial localization, material dimensionality, and the types of defects involved. The most fundamental categorization is based on whether excitons are influenced by the localization potential of crystal defects, dividing them into free excitons and bound excitons. Depending on the binding strength and spatial extension, excitons can be classified into two categories: Wannier–Mott excitons and Frenkel excitons, as shown in Figs. 1(b) and 1(c). Wannier–Mott excitons are characterized by a large exciton Bohr radius (typically several times the unit cell dimension) and a relatively small binding energy (usually ~ 10 meV). In contrast, Frenkel excitons exhibit strong binding characteristics ($E \sim 100$ meV) with an exciton Bohr radius approaching the lattice constant.[41,42] Based on the discussion above, ZnO belongs to the Wannier–Mott exciton, but it has a relatively strong binding property.

3. Exciton luminescence

As a typical third-generation semiconductor material, ZnO exhibits remarkable characteristics of a wide band gap and high exciton binding energy ($\sim$ 60 meV), which confer distinct advantages in light emission applications.[43–45] The luminescence of ZnO comprises band-edge excitonic emission in the ultraviolet region and defect-related emission in the visible region. A thorough grasp of excitonic luminescence processes is essential for clarifying the origin of green emission (primarily arising from defect luminescence), elucidating the mechanisms underlying room-temperature stimulated emission, and promoting the development of high-performance ultraviolet optoelectronic devices. In this section, we summarize the excitonic luminescence properties of ZnO.

3.1. Fluorescence procedure

When the energy of incident photons exceeds the bandgap of ZnO (approximately 3.37 eV at room temperature), valence band electrons are excited to the conduction band, generating electron-hole pairs.[46,47] These high-energy-state carriers subsequently undergo rapid relaxation to the conduction band minimum or valence band maximum through phonon emission (lattice vibrations), preparing for subsequent radiative recombination.[48,49] The room temperature photoluminescence spectrum of ZnO typically consists of NBE free excitonic emission and broadband defect emission covering the visible region (approximately 3.1 eV to 1.653 eV), the latter arising from radiative transitions associated with various intrinsic defects and their complexes in the lattice.[50–52] Figure 2 illustrates the defect energy levels within the ZnO bandgap. Common intrinsic defects include oxygen vacancies (low formation energy, universally present), zinc vacancies (capable of producing two acceptor levels), zinc interstitials (providing shallow donor levels), and oxygen interstitials and antisite defects with higher formation energies. These defects may further combine to form defect clusters such as $V_X Zn_{1-X}$ (with energy levels located at 2.16 eV below the conduction band), thereby significantly affecting the material's electrical conductivity, minority carrier lifetime, and luminescence efficiency. Among these, the origin of the typical green emission band (approximately 2.4–2.5 eV) in undoped ZnO remains controversial; mainstream viewpoints attribute it to transitions from deep donor levels (such as oxygen vacancies or zinc interstitials) to the valence band, or transitions from shallow donor levels to zinc vacancy acceptor levels.[53–55]

Due to the fact that ZnO nanostructures are typically grown in zinc-rich environments, oxygen vacancies and zinc interstitial atoms tend to become the dominant defects. The yellow emission component in ZnO photoluminescence is primarily attributed to radiative transitions induced by oxygen interstitial defects. Specifically, the energy level formed by oxygen interstitial atoms in the band structure is located approximately 2.28 eV below the conduction band; when electrons transition from the conduction band to this level, yellow light is emitted. In ZnO nanorods prepared by wet chemical methods, the generation of yellow emission is likewise associated with oxygen interstitial defects. Notably, through thermal treatment of $Zn(OH)_2$ residues remaining on the surface of ZnO nanostructures or acid treatment of hydroxyl groups, the originally yellow emission can be transformed into green or red luminescence. This indicates that the origin of yellow emission is closely related to the surface chemical state and defect types of the material, while also reflecting the tunability of defect-related luminescence in ZnO.

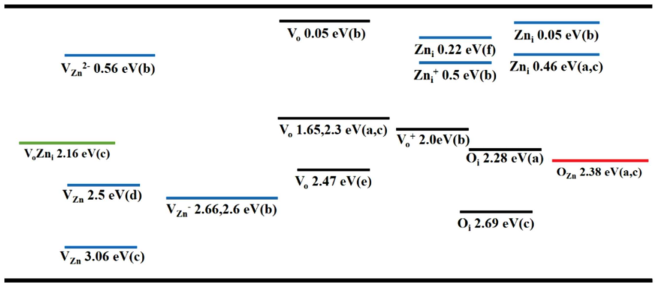


Fig. 2. The defect energy levels of zinc oxide.[56]

Furthermore, in the study of ZnO luminescence, excitation density is a critical factor determining the underlying emission mechanisms. With increasing excitation density, the luminescence mechanism transitions from free exciton recombination and defect-related ordinary spontaneous emission at low densities, to amplified spontaneous emission dominated by exciton–exciton scattering at intermediate densities, and ultimately to stimulated emission resulting from electron–hole plasma (EHP) recombination at high densities. For instance, in ZnO nanoparticles, when the excitation density reaches a threshold of approximately 7.2 GW·cm^{-2}, exciton–exciton scattering becomes the dominant mechanism, driving the luminescence into the amplified spontaneous emission regime characterized by spectral narrowing and threshold behavior.

3.2. Lasing process

Due to the excellent excitonic luminescence properties of ZnO, and based on the stable excitonic emission at room temperature, excitons provide optical gain through interactions such as scattering as the excitation intensity increases.[57–60] Feedback is subsequently obtained in naturally formed micro/nanoscale resonant cavities, ultimately achieving the transition from spontaneous emission to stimulated emission. Common microcavities include random lasing processes, Fabry–Pérot (F-P) lasing processes, and whispering-gallery-mode (WGM) lasers.[61–63]

In arrays of ZnO microrods or disordered particles, light can obtain feedback through multiple scattering, forming random lasers. For instance, ultraviolet random lasing with a peak

wavelength of approximately 391 nm observed in ZnO microrod arrays is realized through this mechanism.[64,65] As shown in Figs. 3(a)–3(c), the natural end facets of ZnO nanowires and nanohexagonal columns can form excellent F-P resonant cavities, wherein light is reflected back and forth between the two end facets and amplified.[66] In this case, lasing with Q over 3000 can be observed. Researchers have also successfully demonstrated surface plasmon polariton lasing with low threshold values and based on the F-P mode in a semiconductor–insulator–metal (SIM) structure composed of ZnO nanowires and metal thin films, which operates at room temperature.[67,68] Compared with others, WGM lasing in ZnO utilizes its hexagonal micro/nanostructures as natural high-Q-factor resonant cavities, achieving optical feedback through total internal reflection. The gain mechanism at the micro/nanoscale may not only follow the conventional EHP process but instead involves richer physics of carrier scattering. In this case, lasing with a Q factor exceeding 6000 was achieved. Advanced spectral testing techniques have made the observation of WGM lasers increasingly easier. As shown in Fig. 3(d), under the influence of the confocal microscope, the excitation light is focused onto the sample, and the laser from the sample is collected and focused onto the detector, and WGM lasing can be obtained (in Fig. 3(e)).[69] Combined with the intrinsic piezoelectric properties of the material or plasmonic effects, ZnO WGM lasers exhibit tremendous potential for realizing low-threshold, tunable miniature ultraviolet lasers.

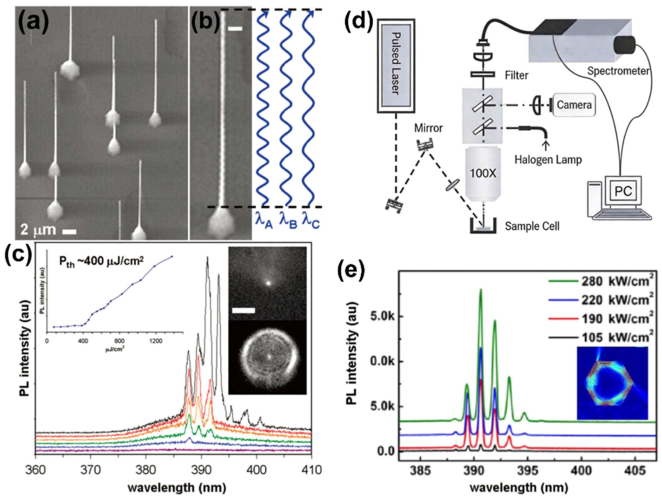


Fig. 3. (a) SEM image of ZnO vertical nanowire cavities grown on sapphire substrate. (b) SEM image of single vertical nanowire with diagram showing Fabry–Perot lasing modes of wavelengths $\lambda_A, \lambda_B, \lambda_C$. Scale bar is 300 nm. (c) Lasing spectra of single ZnO vertical nanowire cavity.[66] (d) The classic micro-area spectroscopy system. (e) ZnO whispering gallery mode under different pump power densities.[69]

4. Exciton-related interactions

As a typical third-generation semiconductor material, ZnO has the remarkable characteristics of a wide band gap and high exciton binding energy, which makes it have obvious advantages in the construction of light-emitting devices, especially UV lasers.[61,70,71] Because of this feature, the coupling between excitons and other particles (such as exciton–exciton, exciton–photon, exciton–phonon, exciton–plasmon, etc.) presents a wealth of physical phenomena. In this section, we summarize several exciton-related interactions and explore their spectral performance and potential physical mechanisms.

4.1. Exciton–exciton interaction

At room temperature, the fluorescence spectra of ZnO primarily exhibit a UV NBE emission located at about 380 nm. In fluorescence spectroscopy experiments, the UV NBE emission behavior of ZnO is influenced by the intensity of the pumping light. Under low power density pumping conditions, the UV NBE emission of ZnO is dominated by free exciton recombination radiation. As the pumping power density increases, the exciton concentration in ZnO also increases. Due to the predominance of exciton–exciton scattering interactions, the continuous spectrum formed by exciton–exciton collisions measured in the experiment is referred to as the P-band.[72] This results in a red shift of 99 meV in the fluorescence emission peak compared to the free exciton radiation peak. When the pumping power density continues to increase and the exciton concentration exceeds the critical Mott phase transition concentration, the interactions between excitons intensify, forming an EHP, which exhibits physical characteristics completely different from exciton radiation. Figures 4(a) and 4(b) visually illustrate the mechanism of NBE emission in ZnO under different carrier concentrations.[73] Compared to that of exciton transitions (greater than 5 ps), EHP transitions have a shorter rise and decay time due to their rapid thermalization (less than 100 fs). The dynamic differences between the two can be revealed in depth through ultrafast spectroscopy techniques such as time-resolved spectroscopy and transient absorption spectroscopy. Hendry *et al.*[74] utilized optical pump–terahertz probe techniques to reveal the formation process of EHP in ZnO single crystals. Under low pumping power densities, hot electron–hole gas slowly cools down after 10–100 ps to form excitons, overturning the traditional view of "rapid formation of hot excitons". When the exciton concentration exceeds the Mott phase transition, the plasma rapidly decays to near the Mott density within 1.5 ps through Auger recombination and tends to stabilize, a process of which is independent of lattice temperature and occurs before carrier cooling. This technique directly observes exciton formation dynamics for the first time by distinguishing the characteristic conductivity responses of free carriers and excitons, which is of great significance for understanding the carrier behavior of ZnO under high-density excitation (such as in laser applications). Versteegh *et al.*[75]

pointed out that the lasing in ZnO nanowires at room temperature is not of excitonic nature, as is often thought, but instead is electron–hole plasma lasing. On the other hand, EHP can also lead to bandgap renormalization, causing the conduction band edge to shift downward and the valence band edge to shift upward. Consequently, a significant red shift of the fluorescence peak position with varying pumping power is observed in experiments, as illustrated in Fig. 4(c).

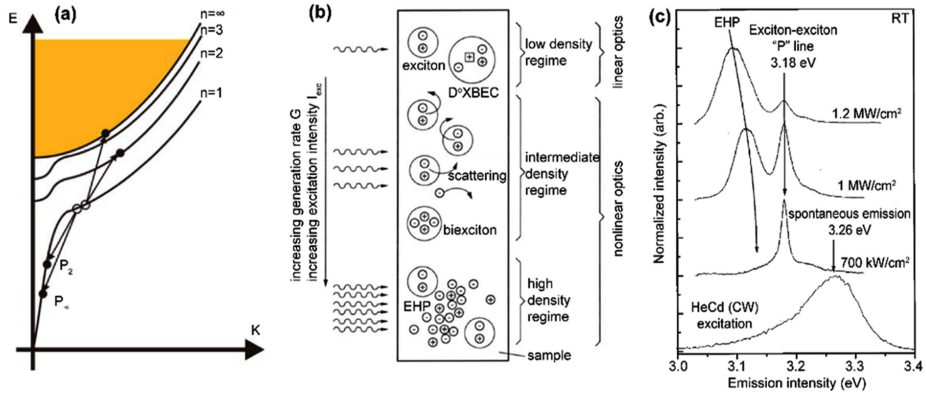


Fig. 4. (a) Schematic drawing of the inelastic exciton–exciton scattering process and (b) the scenario in a semiconductor with increasing excitation.[73] (c) Normalized PL spectra for various excitation intensities at room temperature.[72]

4.2. Exciton–photon interaction

The exciton-polariton, formed by the strong coupling of excitons and photons in ZnO, is a quasi-particle possessing both particle and photon properties. It is also crucial for realizing cutting-edge physical phenomena such as low-threshold lasers[76] and Bose–Einstein condensation,[77,78] as well as novel optoelectronic devices[79] (e.g., ultrafast optical switches and single-photon sources). Compared to narrow-bandgap semiconductor materials like CdTe and GaAs, ZnO stands out as an ideal material for realizing exciton-polaritons at room temperature due to its high exciton binding energy (60 meV), which leads to a relatively stable strong coupling between excitons and optical cavity modes at room temperature. In 2006, Vugt *et al.*[80] investigated

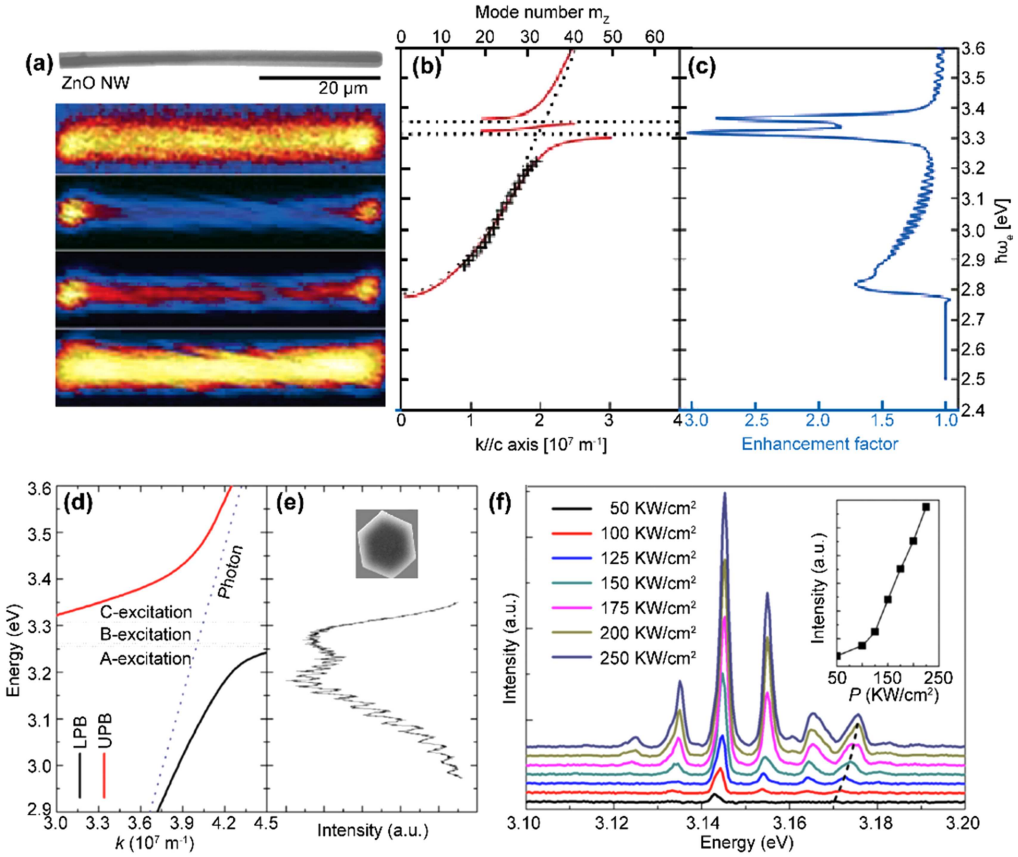


Fig. 5. (a) TEM image and spatially resolved excitation images of ZnO taken at different emission energies, (b) numerical simulation of exciton polariton dispersion spectrum, (c) emission intensity enhancement factor at the tip.[80] (d) The numerical exciton-polaritons dispersion curve and (e) TE polarized μ-PL spectrum of ZnO microrod with a diameter of 9.38 μm, (f) the lasing spectra under different pumping power densities.[82]

optical cavity mode radiation in a single ZnO nanowire using two-photon non-resonant excitation. As show in Fig. 5(a), two enhanced fluorescence emission bands in the ultraviolet region were discovered in the fluorescence spectrum collected from the tip of the ZnO rod. The enhancement factor, defined as the ratio of emission intensity at the tip to that at the body of the rod, exhibited a series of resonance peaks in the 3.0–3.2 eV range, attributed to the F-P cavity modes formed by light reflection and oscillation at the two ends of the nanorod. Furthermore, by utilizing the exciton-polariton dispersion curve of ZnO (as shown in Fig. 5(b)) and the F-P cavity mode formula, they simulated the F-P resonance modes of exciton-polaritons in the nanorod (represented by the black cross in the 2.8–3.2 eV region in Fig. 5(b)). The numerical simulation results of exciton-polariton resonance modes reveal two enhanced emission peaks at the bottom of the upper branch and the top of the lower branch of exciton-polaritons, respectively. The positions of these two enhanced emission peaks align with the two ultraviolet emission bands observed in the fluorescence experiment, indicating the realization of exciton-polaritons in ZnO nanorods shown in Fig. 5(c). Chen's group[81] discovered the phenomenon of whispering gallery mode radiation in the tapered arm of the ZnO tetrapod with gradually decreasing diameter. Scanning microscopy fluorescence spectroscopy measurements revealed that as the cavity gradually narrowed, the whispering gallery cavity modes gradually shifted to the blue, thereby approximating the energy of ZnO excitons and coupling with them. The linearly decreasing blue shift of whispering gallery modes in the cavity, simulated using exciton-polariton dispersion, fully aligns with experimental results, thus indicating the generation of effective whispering gallery mode exciton-polaritons in the cavity. In 2011, our research group[82] achieved low-threshold room-temperature exciton-polariton lasing using hexagonal ZnO microcavities, and observed a Rabi splitting energy of 90 meV and a nonlinear blue shift phenomenon, as shown in Figs. 5(d)–5(f).

4.3. Exciton–phonon interaction

The exciton–phonon interaction in ZnO is a crucial component of its light emission physical process, playing a pivotal role in understanding its UV emission characteristics and designing optoelectronic devices.[83–86] This interaction primarily occurs through the coupling between excitons and lattice vibrations (phonons), significantly influencing the shape, position, and dynamics of the emission peaks. By utilizing low-temperature spectroscopic testing techniques, one can clearly observe the exciton recombination in ZnO and their corresponding phonon replicas formed by the coupling between excitons and lattice vibrations (phonons). As shown in Fig. 6, the variable-temperature photoluminescence spectra of ZnO nanorods using low-temperature spectroscopic techniques have been measured.[87] When the temperature is below 30 K, the UV fluorescence spectrum primarily consists of the emission peaks of bound exciton (BX) with an energy of 3.367 eV, free exciton (FX) with an energy of 3.377 eV, and their corresponding phonon replicas. According to previous reports, the energies of longitudinal optical (LO) and transverse optical (TO) phonon modes are 70 meV and 52 meV, respectively. Consequently, the five peaks located at 3.321 eV, 3.296 eV, 3.245 eV, 3.226 eV, and 3.173 eV correspond to FX-TO, BX-LO, FX-TO-LO, BX-2LO, and FX-TO-2LO, respectively. As the temperature gradually increases, more and more BXs are thermally activated and convert to FXs. The peaks of BX and its phonon replicas gradually disappear, while the relative intensities of the FX emission as well as its phonon replicas gradually strengthen and eventually become dominant in the RT-PL spectra. Therefore, as the temperature rises to room temperature, the NBE emission in the ultraviolet region of ZnO is composed of the peaks of free excitons and their phonon replicas, which usually shows the characteristics of spectral line broadening and red shift.

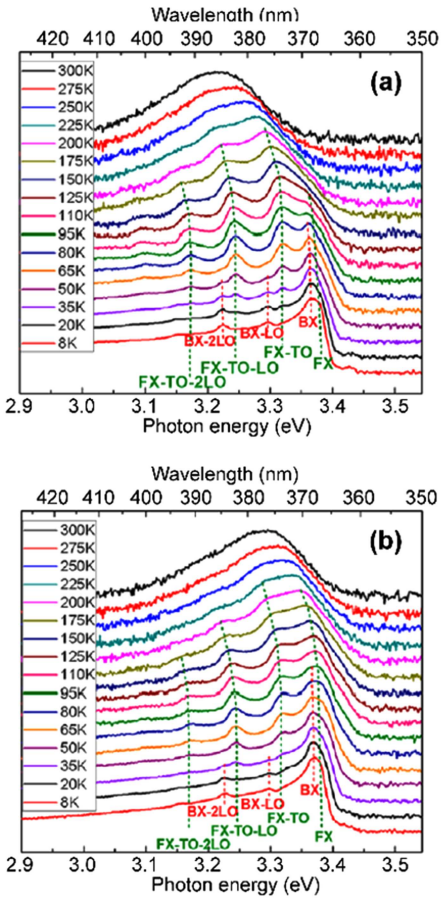


Fig. 6. Temperature-dependent PL spectra of ZnO nanorod arrays with different diameters.[87]

4.4. Exciton–plasmon interaction

With the continuous development of laser technology, its miniaturization has also garnered widespread attention. Due to the limitation of optical diffraction, the physical size of tra-

ditional laser sources is at least half the wavelength of light, severely restricting their miniaturization.[88] To address this challenge, Bergman and Stockman[89] proposed a novel concept of laser in 2003, introducing metals and semiconductors into nanoscale systems. Through efficient coupling between exciton luminescence in semiconductors and plasmonic modes on metal surfaces, photonic oscillations are converted into electronic oscillations, enabling them to be free from the constraints of cavity size. This results in surface plasmon amplification by stimulated emission of radiation (Spaser), a plasmonic nanolaser with dimensions as small as $\sim$ 10 nm. This composite resonant cavity plasmonic nanolaser, composed of metal, insulating medium, and semiconductor gain medium, was first reported experimentally in 2009.[90–92] The physical advantage of high exciton binding energy in ZnO also provides sufficient optical gain to compensate for metal ohmic losses. In 2014, R. F. Oulton *et al.*[93] constructed a composite laser microcavity with SPP coupling using ZnO nanowires and metal Ag film, as shown in Figs. 7(a)–7(c). The dynamic processes of two laser modes were systematically investigated by using pump-probe technology, and it was found that the spontaneous emission recombination rate of the ZnO/Ag composite system was significantly enhanced, with lasing pulse times as low as 800 fs. In 2015, Chou *et al.*[94] constructed a ZnO/Ag composite structure microcavity, as shown in Figs. 7(d)–7(f). Under low temperature conditions, the distinct mode structure plasmonic lasing using Ag-SPP coupled ZnO nanorods was observed. Time-resolved spectroscopy measurements showed a significant increase in exciton recombination rate in this composite microcavity, with a Purcell factor as high as 20.4. The research results indicated that the introduction of Ag-SPP promoted the transition of electrons from the conduction band to the valence band. In 2017, our group[95] constructed a composite laser microcavity with SPP coupling using ZnO nanowires and metal Ag film, achieving room-temperature operation of subwavelength-scale plasmonic nanolasers. And the physical mechanism of blue shift in this type of laser mode was systematically clarified.

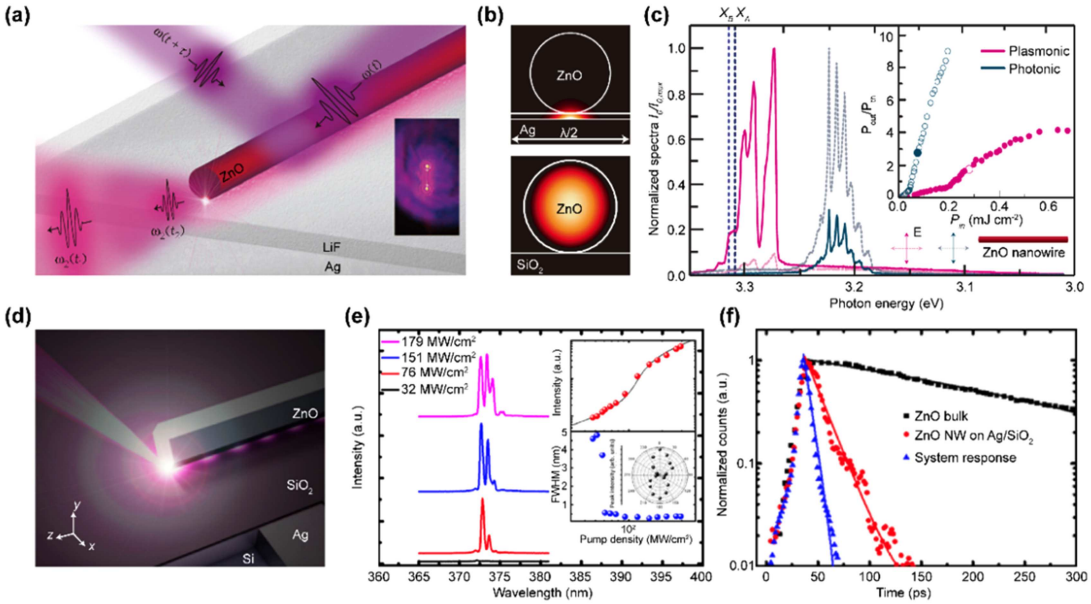


Fig. 7. (a) Schematic of the geometry and the emission of a ZnO nanowire optically excited with two time-delayed (τ) pump pulses. (b) Calculated nanowire modes for plasmonic and photonics devices respectively. (c) Comparison of the measured emission near twice the threshold from a selected plasmonic nanowire ($\sim$ 150 nm) and a thicker ($\sim$ 250 nm) photonic nanowire on a quartz substrate.[93] (d) Schematic bird's eye view diagram of the device. (e) Measured spectra at the laser pumping power density from 32 MW/cm^2 to 179 MW/cm^2 inserted with light–light curve and FWHM versus the pumping power density. (f) Time-resolved PL signals (dots) and fitted curves (solid lines) at 77 K.[94]

5. Application

5.1. Optoelectronic devices

With its excellent physical properties and outstanding exciton recombination luminescence, ZnO is one of the ideal candidate materials for developing ultraviolet LEDs and LDs. Over the past two decades, ZnO-based electroluminescent devices have been a focal point in semiconductor research. However, achieving stable and high-quality p-type doping in ZnO remains a bottleneck difficulty, primarily due to factors including the low solubility of acceptor impurities, deep acceptor levels (high ionization energy), and a strong self-compensation effect. Consequently, it has become an optional scheme to construct ZnO-based heterojunction structures by employing other p-type materials to realize effective hole injection (such as p-Si, p-GaN, and p-AlGaN), which has received widespread attention from researchers. In this structure, electrons and holes are injected from the n-ZnO and the p-type layer, respectively, and recombined in the active region within the ZnO layer or at the heterojunction interface to form excitons, thereby generating luminescence.

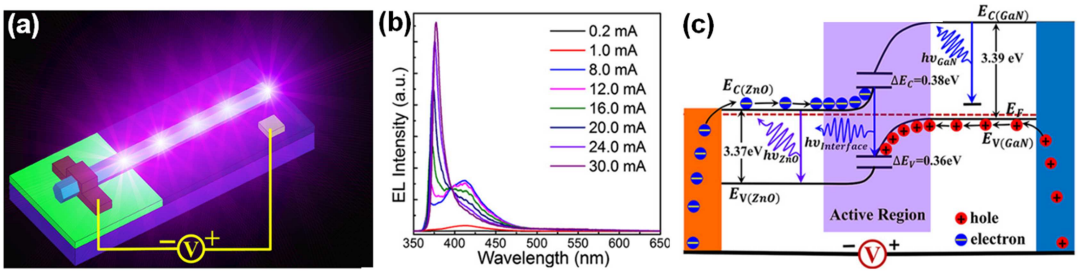


Fig. 8. An n-ZnO microwire/p-GaN heterojunction:[96] (a) schematic diagram of the device; (b) the EL spectra driven by different currents; (c) the energy band structure diagram.

ZnO exciton luminescence in LEDs Because of the similar crystal structure to ZnO, close lattice constants, and low lattice mismatch (1.9%),[97–99] p-GaN has become an ideal hole injection material to construct the heterojunctions with ZnO. Besides, ZnO and GaN have similar bandgaps of 3.37 eV and 3.4 eV, respectively. In 2009, Wang's group achieved the high brightness blue LEDs in the n-ZnO nanowires/p-GaN substrate mainly in the wavelength range between 400–440 nm, and the luminescent center showed the blue shifting through increasing the injection current.[100] Next year, Oleg *et al.*[101] constructed the n-ZnO nanowire arrays/p-GaN epitaxial layers LED with a narrow UV emission peak centered at 397 nm which was stable with increased driven voltage. In 2017, Jiang *et al.*[96] reported a heterojunction LED based on n-ZnO microrod in Fig. 8(a), which presented the different EL spectra under various injection currents. As shown in Fig. 8(b), with the low driven current, the device emitted the violet-blue wavelength range light with the center at 412 nm. When the driven current became higher, there was an emission peak at 370 nm generating. Lots of reports showed the similar results that the n-ZnO/p-GaN heterojunction LEDs had the wide emission wavelength range EL performance.[102,103] According to the energy band schematic in Fig. 8(c), these emissions can be attributed to the band-edge emission of the ZnO MW, the transition from the shallow donor level in GaN to the Mg doping-related acceptor level, and the radiative recombination of electrons from the ZnO MW conduction band with holes from the GaN valence band at the heterojunction interface.[104–107] In addition, ZnO and GaN show similar refractive index and crystal structure, which can cause serious optical and electrical loss at the interface. Therefore, the design of the heterojunction interface engineering and the optimization of the energy band structure are critical for enhancing the device luminescence efficiency, stability, and spectral monochromaticity of n-ZnO/p-GaN LEDs.

In order to improve the exciton recombination luminescent efficiency, the electron blocking layer is widely regarded as an effective means. It can optimize the energy band structure and interface loss, and effectively suppress the electron in ZnO transferring into the GaN conduction band, thereby improving the NBE emission in ZnO. In 2007, Chen *et al.*[108] introduced a SiO_2 layer in the n-ZnO/p-GaN to obtain a sharp emission peak at 394 nm, which was attributed to the recombination of accumulated carriers between n-ZnO/SiO_2 and p-GaN/SiO_2 junctions. In 2012, Liu *et al.*[109] introduced a Ga_2O_3 layer in the planar n-ZnO/p-GaN heterojunction device to effectively block carriers for radiative recombination in ZnO, finally realizing the strong UV emission at $\sim$ 392 nm. The next year, Wang *et al.*[110] illustrated that the Al_2O_3 layer was inserted in the heterojunction device to realize the violet emission in n-ZnO. Next, in 2017, Liu's group[111] demonstrated a $\sim$ 30-fold improvement of near-UV EL intensity by inserting a thin Al_2O_3 dielectric retarding layer into the ZnO quantum dots side, in which the electrons injected from ZnO were effectively slowed and detained in the ZnO quantum dots emissive layer, as seen in Fig. 9(a). Besides, the dielectric materials of MgF_2[112] and MgO[113] were also demonstrated to effectively block the electron in ZnO to improve the near-band-edge recombination emission. And the high-k materials (a dielectric constant of 25–30) of HfO_2 with a modest band gap (5.8–6.0 eV) could be a good electron blocking and hole transporting layer for the n-ZnO/p-GaN LED device, in which the conduction-band offsets of HfO_2/ZnO and valence-band offsets of HfO_2/GaN were calculated as $\sim$ 2.29 eV and $\sim$ 0.3 eV.[114,115] Fang's group[116,117] reported the improvement of violet emission in ZnO and narrowed emission peak, which resulted from the enhanced radiative center recombinations with inserting HfO_2 layer. In addition, Zhang *et al.*[118] reported that the utilization of ZnS as an intermediate layer can lower the barrier height for holes and keep the effective electron blocking to exhibit UV emission. Sun *et al.*[119] reported that the MgZnO layer also could confine the injection carriers to increase the excitonic emission intensity in the ZnO active region.

With the widest direct band gap of 6.2 eV, AlN has good lattice match with ZnO and GaN, which can be an ideal interface modification layer to improve the performance of n-ZnO/p-GaN heterojunction LEDs.[120,121] In recent years, our group also introduced an AlN layer in the n-ZnO nanorods/p-GaN LEDs to obtain pure UV emission.[122] According to the calculated results, the valence band offset between AlN and GaN was 0.34 eV, and the conduction band offset between AlN

and ZnO was 3.28 eV. Thus, the electron–hole recombination could take place in the ZnO layer to realize more exciton luminescence. As presented in Fig. 9(b), the n-ZnO nanorods/AlN-coated p-GaN wafer heterojunction displayed a pure UV EL spectrum that was almost completely coincident with the ZnO PL spectrum. The snapshot in the inset of Fig. 9(b) illustrated the bright UV emission of the optimized device. After that, the ZnO/AlN core-shell nanoarrays were constructed into a heterojunction device with a p-GaN substrate.[123] The perfect ZnO/AlN core-shell structure resulted in effective surface defect passivation, thus effectively improving the inter-band recombination of ZnO. Moreover, the AlN shell with an optimized thickness could form a suitable energy-band configuration with a high electron barrier to prevent electron injection from ZnO to GaN. Consequently, a pure and narrow UV emission peak centered at 382 nm was achieved in the heterojunction device, as can be seen in Fig. 9(c). All the results demonstrated that a suitable energy band structure and interface engineering can improve the exciton recombination luminescence of ZnO in the heterojunction devices to obtain pure and bright UV light-emitting devices.

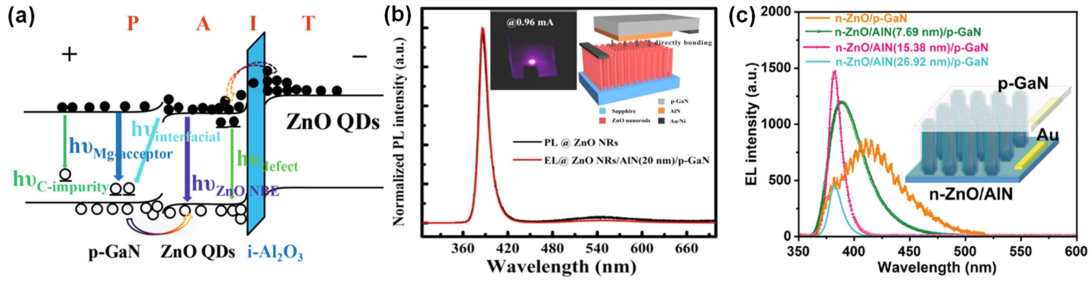


Fig. 9. (a) The energy band structure diagram of n-ZnO/i-Al_2O_3/n-ZnO/p-GaN heterojunction device.[111] (b) The EL spectra of n-ZnO/i-AlN/p-GaN heterojunction device, insets are the driven device snapshot and schematic diagram of the device structure.[122] (c) The EL spectra of different devices including n-ZnO/p-GaN and the ZnO–AlN core–shell/p-GaN with different AlN shell thicknesses, insets are the schematic diagrams of the device structure.[123]

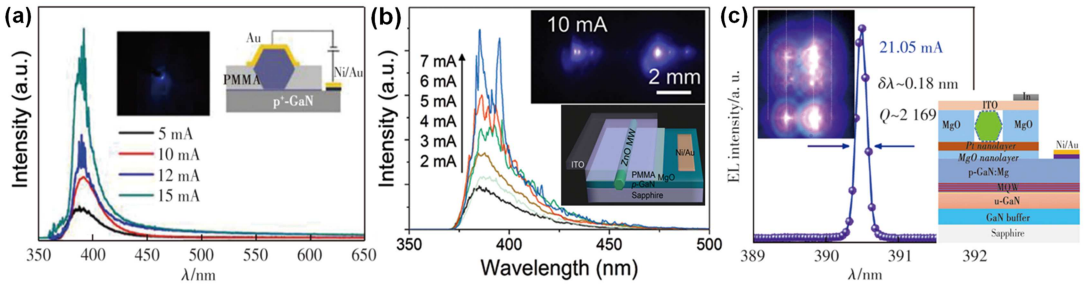


Fig. 10. The EL spectra of (a) ZnO/p-GaN device,[71] (b) ZnO/MgO/p-GaN device,[124] and (c) ZnO/Pt NPs decorated MgO/p-GaN device.[125] Insets are the snapshots of the driven devices and the device structure diagrams.

ZnO exciton lasing in LDs Compared to LEDs, LDs require higher current density and injection efficiency. In 2009, Ma *et al.*[126] demonstrated that the electrically pumped random exciton lasing was achieved in the Au/SiO_2/ZnO nanorods array formed metal–insulator–semiconductor structures under sufficiently high driven voltage, which was generated from the population inversion in ZnO and the multiple scattering. The next year, Shan's group[127] obtained stable and low threshold random lasing in the Au/i-ZnO/MgO/n-ZnO structure devices. Following this, efforts were made to realize exciton lasing with well-defined modes in ZnO-based heterojunction diodes. In 2011, our group[71] constructed the ZnO microrod/p-GaN heterojunction bonded by a ZnO buffer layer, and observed the electrically driven WGM lasing under high injection current, as shown in Fig. 10(a). The transformation from spontaneous emission to stimulated emission process with various resonance peaks was obvious with the increased driven current. Furthermore, Yang *et al.* constructed Van der Waals heterojunction of Ag film coated ZnO microwire/i-MgO/p-GaN device which achieved the stimulated emission in the UV region, as shown in Fig. 10(b). The high conductivity and reflectivity of Ag film improved the current injection efficiency and lasing directionality. In 2022, our group[128] designed the nanolaser based on the individual ZnO nanorod and p-GaN wafer, further introducing the PEDOT and HfO_2 layer to form the step-shaped band structure arrangement to improve the carriers injection and radiation recombination efficiency. Finally, the single mode exciton lasing with a narrow peak (linewidth of 1.4 nm) was realized. In addition, Zhou *et al.*[125] reported the electrically pumped single mode lasing in the Pt nanoparticles (NPs)@ZnO microwire/Pt/MgO/p-GaN heterojunction device, as displayed in Fig. 10(c). Among them, the Pt NPs decorated on ZnO microwire exhibited excellent light absorption, the MgO layer modified the heterojunction energy band, and the Pt layer improved the carriers injection efficiency. Hence, the single mode lasing was achieved with high

performance, including peak center at ∼ 390.5 nm, linewidth of ∼ 0.18 nm and Q factor of ∼ 2169. Furthermore, Jiang's group constructed different double-heterojunctions to realize high quality lasers, such as n-AlGaN/n-ZnO/Pt/MgO/p-GaN device,[129] n-AlGaN/SnO_2/n-Pt NPs@ZnO/Pt/MgO/p-GaN device.[130] Consequently, the exciton lasing in the electrically pumped heterojunction devices showed the high performance in different structured devices, which demonstrated the development and application potential of ZnO-based UV LDs.

5.2. Lasing sensors

Based on the wurtzite structure, which lacks the center of inversion, ZnO crystal exhibits the piezoelectric effect in addition to the thermo-optic effect, electro-optic effect, etc. Subject to changes in ambient temperature, electric field, and applied stress, the refractive index and the polarization field will change. Moreover, the WGM lasing can achieve highly sensitive sensing with its high monochromaticity and super narrow linewidth. Consequently, a simple and miniaturized sensor can be realized on the basis of ZnO micro-laser. For instance, our group[131] realized a temperature sensor based on the individual Ga-doped ZnO WGM microresonator, which has a conductivity of ∼ 1.75 S/cm and a thermo-optic coefficient of 16.7×10^{-4} K^{-1} around the bandgap energy of ZnO. As shown in Fig. 11(a), the WGM lasing mode with a tuning range of 2 nm was achieved by the effect of current-induced temperature rising, which changed the refractive index of the crystal. In addition, Wang's group[132] obtained a strain sensor based on the single ZnO WGM laser. As presented in Fig. 11(b), there was a shift of the strain-mediated lasing mode that was occupied by the piezoelectric polarization effect of the ZnO microwire. In 2022, our group[133] demonstrated the electric field influenced ZnO WGM lasing mode shifting, and the ZnO microrod had the electro-optic coefficient and Kerr electro-optic constant of 7.68×10^{-9} m/V and 5.17×10^{-10} m·V^{-2} near the bandgap energy. The above reports illustrated the potential of ZnO micro-laser in the application region of high-sensitive sensors.

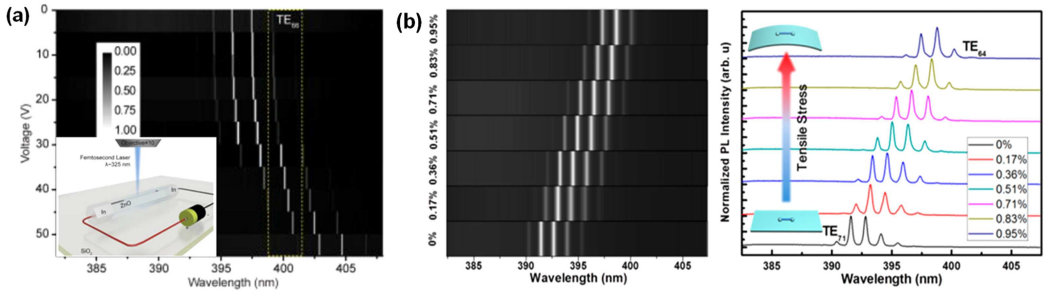


Fig. 11. ZnO WGM lasing sensors. (a) The 2D images of lasing spectra under different bias voltages.[131] (b) The lasing spectra and its 2D images under different degrees of bending.[132]

6. Conclusion and perspectives

In conclusion, this review offers a systematic summary of the fundamental concepts, classification frameworks, and luminescence mechanisms in exciton physics, with a specific emphasis on ZnO as a representative material system. It not only explores exciton-related luminescence properties, particularly lasing behavior in ZnO micro/nanostructures, but also discusses the diverse interactions between ZnO excitons and other elementary excitations and quasiparticles, including excitons, photons, phonons, and surface plasmons, along with their influence on recombination dynamics. Furthermore, various applications of ZnO exciton recombination luminescence are discussed and illustrated, encompassing ultraviolet light-emitting devices and laser sensors. Despite the longstanding challenge of achieving effective p-type doping in ZnO, a major bottleneck for its broader application, the material continues to exhibit outstanding excitonic emission properties, rich physical phenomena, and significant potential across multiple fields. For example, applications in lasing, sensors, transition layers for optoelectronic devices, flexible optoelectronic devices, and low-dimensional materials all show promising prospects and expectations. Undoubtedly, understanding and engineering defects in ZnO remain crucial scientific pursuits that demand sustained research efforts. Although substantial challenges persist, the remarkable physical properties and vast application prospects of ZnO materials will continue to motivate extensive investigation worldwide, driving the field toward greater maturity and impact. Future research is expected to further bridge fundamental physical insights with the development of advanced functional devices, fostering continued innovation in both science and technology.

Acknowledgement

This work was supported by the National Natural Science Foundation of China (Grant Nos. 62404040, 52595642, 62375049, and 52572172).

References

[1] Ivanov A L, Haug H and Keldysh L V 1998 *Phys. Rep.* **296** 237

[2] Mikhnenko O V, Blom P W M and Nguyen T Q 2015 *Energy Environ. Sci.* **8** 1867
[3] Jiang Z J, Ren A, Yan Y L, Yao J N and Zhao Y S 2022 *Adv. Mater.* **34** 2106095
[4] Axt V M and Mukamel S 1998 *Rev. Mod. Phys.* **70** 145
[5] Klimov V I 2007 *Annu. Rev. Phys. Chem.* **58** 635
[6] Wheeler D A and Zhang J Z 2013 *Adv. Mater.* **25** 2878
[7] Kumar V, Nisika and Kumar M 2021 *Adv. Opt. Mater.* **9** 2001150
[8] Dimitriev O P 2022 *Chem. Rev.* **122** 8487
[9] Regan E C, Wang D Q, Paik E Y, Zeng Y X, Zhang L, Zhu J H, MacDonald A H, Deng H and Wang F 2022 *Nat. Rev. Mater.* **7** 778
[10] Ozgür U, Alivov Y I, Liu C, Teke A, Reshchikov M A, Dogan S, Avrutin V, Cho S J and Morkoç H 2005 *J. Appl. Phys.* **98** 041301
[11] Klingshirn C 2007 *ChemPhysChem* **8** 782
[12] Klingshirn C, Fallert J, Zhou H, Sartor J, Thiele C, Maier-Flaig F, Schneider D and Kalt H 2010 *Phys. Status Solidi B* **247** 1424
[13] Choi Y S, Kang J W, Hwang D K and Park S J 2010 *IEEE Trans. Electron Devices* **57** 26
[14] Lai Y Y, Lan Y P and Lu T C 2013 *Light Sci. Appl.* **2** e76
[15] Panda D and Tseng T Y 2013 *J. Mater. Sci.* **48** 6849
[16] Lu Y J, Shi Z F, Shan C X and Shen D Z 2017 *Chin. Phys. B* **26** 047703
[17] Xu Z X, Zhang Y L and Wang Z N 2019 *J. Phys. D* **52** 223001
[18] Liu J J, Zhong Q L, Wu C, Chen Z B, Yu X M, Yu X, Zhang H, Cao Y, Li Z H, Qiao Q and Zhou Y T 2025 *Micro Nanostruct.* **201** 208105
[19] Singh M, Zakria M, Pannu A S, Sonar P, Smith C, Mahasivam S, Ramanathan R, Tran K, Tawfik S, Murdoch B J, Mayes E L H, Spencer M J S, Phillips M R, Bansal V and Ton-That C 2024 *ACS Nano* **18** 16947
[20] Wang J P, Yang H Y and Yang P 2022 *Compos. B Eng.* **233** 109645
[21] Chen X H, Veettil B P and Nasiri N 2025 *Nano Today* **63** 102754
[22] Li Z Y, Luo H X and Chen T Y 2026 *Crystals* **16** 65
[23] Murzin S P 2025 *Processes* **13** 3755
[24] Zubiaga A, García J A, Plazaola F, Muñoz-Sanjosé V and Martínez-Tomás M C 2002 *J. Appl. Phys.* **92** 7330
[25] Banerjee D, Sankaranarayanan S, Khachariya D, Nadar M B, Ganguly S and Saha D 2016 *Appl. Phys. Lett.* **109** 031111
[26] Guo S H, Mihalyi-Koch W, Mao Y H, Li X Y, Bu K J, Hong H L, Hautzinger M P, Luo H, Wang D, Gu J Z, Zhang Y F, Zhang D Z, Hu Q Y, Ding Y, Yang W E, Fu Y P, Jin S and Lü X J 2024 *Nat. Commun.* **15** 3001
[27] Mott N F 1938 *Proc. R. Soc. Lond. Ser. A Math. Phys. Sci.* **167** 0384
[28] Wannier G H 1937 *Phys. Rev.* **52** 0191
[29] Ghosh S, Su R, Zhao J, Fieramosca A, Wu J, Li T, Zhang Q, Li F, Chen Z and Liew T J P I 2022 *Photon. Insights* **1** R04
[30] Tavkhelidze A, Jangidze L, Skhiladze G, Sikharulidze S, Dzneladze K, Kvesitadze R and Bibilashvili A J N 2024 *Nanomaterials* **14** 1889
[31] Mujahid M, Gradauskas J, Suziedelis A, Sirmulis E and Asmontas S 2025 *Energies* **18** 3543
[32] Li J G, Yang R D, Li R X and Grigoropoulos C P 2025 *Adv. Opt. Mater.* **13** 2403137
[33] Yang B and Han K L 2021 *J. Phys. Chem. Lett.* **12** 8256
[34] Khalfin S and Bekenstein Y 2019 *Nanoscale* **11** 8665
[35] Li S R, Luo J J, Liu J and Tang J 2019 *J. Phys. Chem. Lett.* **10** 1999
[36] Lv C F, Yang X G, Wu Y R, Lei F H, Liang Y C, Yang D W, Sui L Z, Qin J X, Wu Q L, Lai S L, Liu H, Zang J H, Cheng S B, Liu K K and Shan C X 2025 *Nat. Commun.* **16** 1913
[37] Choi B, Alfieri A D, Chen W and Jariwala D 2026 *Adv. Funct. Mater.* **36** e31054
[38] Kan C X, Wu Y T, Xu J, Wan P and Jiang M M 2021 *Opt. Express* **29** 1023
[39] Tanaka K and Kondo T 2003 *Sci. Technol. Adv. Mater.* **4** 599
[40] Lin Y X, Ling X, Yu L L, Huang S X, Hsu A L, Lee Y H, Kong J, Dresselhaus M S and Palacios T 2014 *Nano Lett.* **14** 5569
[41] Kim H, Hyun D, Hilal M, Cai Z C and Moon C W 2024 *Electronics* **13** 3572
[42] Shekhar S, Bogaerts W, Chrostowski L, Bowers J E, Hochberg M, Soref R and Shastri B J 2024 *Nat. Commun.* **15** 751
[43] Galdámez-Martinez A, Santana G, Güell F, Martínez-Alanis P R and Dutt A 2020 *Nanomaterials* **10** 857
[44] Janotti A and Van de Walle C G 2009 *Rep. Prog. Phys.* **72** 126501
[45] Liu M S, Jiang M M, Zhao Q Z, Tang K, Sha S L, Li B H, Kan C X and Shi D N 2023 *ACS Appl. Mater. Interfaces* **15** 13258
[46] Anpo M and Kubokawa Y 1984 *J. Phys. Chem.* **88** 5556
[47] Meyer B K, Alves H, Hofmann D M, Kriegseis W, Forster D, Bertram F, Christen J, Hoffmann A, Strassburg M, Dworzak M, Haboeck U and Rodina A V 2004 *Phys. Status Solidi B* **241** 231
[48] Zhukov V P, Tyuterev V G and Chulkov E V 2012 *J. Phys.: Condens. Matter* **24** 405802
[49] Bauer C, Boschloo G, Mukhtar E and Hagfeldt A 2004 *Chem. Phys. Lett.* **387** 176
[50] Wang M S, Zhou Y J, Zhang Y P, Kim E J, Hahn S H and Seong S G 2012 *Appl. Phys. Lett.* **100** 101906
[51] Wang Y G, Lau S P, Zhang X H, Hng H H, Lee H W, Yu S F and Tay B K 2003 *J. Cryst. Growth* **259** 335
[52] Ravi K and Biroju P K G 2017 *J. Appl. Phys.* **122** 044302
[53] Tam K H, Cheung C K, Leung Y H, Djurisic A B, Ling C C, Beling C D, Fung S, Kwok W M, Chan W K, Phillips D L, Ding L and Ge W K 2006 *J. Phys. Chem. B* **110** 20865
[54] Djurisic A B, Leung Y H, Tam K H, Ding L, Ge W K, Chen H Y and Gwo S 2006 *Appl. Phys. Lett.* **88** 103107
[55] Vanheusden K, Seager C H, Warren W L, Tallant D R and Voigt J A 1996 *Appl. Phys. Lett.* **68** 403
[56] Lu J F, Dai J, Liu W, Wang X X, Qin F F, Wang R, Shi Z L, Zhu G Y and Xu C X 2025 *Construction and Characterization of ZnO Micro/Nanolasers, in Optical Characterization of Microstructures and Optoelectronic Devices Based on Wide Band Gap Semiconductors*, ed. Xu S J (Singapore: Springer) pp. 181–233
[57] Matsuzaki R, Soma H, Fukuoka K, Kodama K, Asahara A, Suemoto T, Adachi Y and Uchino T 2017 *Phys. Rev. B* **96** 125306
[58] Klingshirn C, Hauschild R, Fallert J and Kalt H 2007 *Phys. Rev. B* **75** 115203
[59] Tarasov A P, Muslimov A E and Kanevsky V M 2022 *Materials* **15** 8723
[60] Liu M S, Sha S L, Xi Z Y, Tang K, Wan P, Kan C X, Shi D N and Jiang M M 2026 *J. Mater. Sci. Technol.* **243** 89
[61] Li J T, Lin Y, Lu J F, Xu C X, Wang Y Y, Shi Z L and Dai J 2015 *ACS Nano* **9** 6794
[62] Gargas D J, Moore M C, Ni A, Chang S W, Zhang Z Y, Chuang S L and Yang P D 2010 *ACS Nano* **4** 3270
[63] Chen Y T and Chen Y F 2011 *Opt. Express* **19** 8728
[64] Tarasov A P, Zadorozhnaya L A and Kanevsky V M 2024 *J. Appl. Phys.* **136** 073102
[65] Yao X R, Li H Q, Li Z Q, Huang X P, Zhao Y S, Liu X X, Zhu P W, Liu B B, Cui T, Sun C and Bao Y J 2020 *J. Phys. Chem. C* **124** 7523
[66] Gargas D J, Toimil-Molares M E and Yang P D 2009 *J. Am. Chem. Soc.* **131** 2125
[67] Xu L T, Li F, Liu Y H, Yao F Q and Liu S 2019 *Appl. Sci.-Basel* **9** 861
[68] Repp D, Barreda A, Vitale F, Staude I, Peschel U, Ronning C and Pertsch T 2023 *Opt. Express* **31** 3364
[69] Wang Y Y, Qin F F, Lu J F, Li J T, Zhu Z, Zhu Q X, Zhu Y, Shi Z L and Xu C X 2017 *Nano Res.* **10** 3447
[70] Pan C F, Dong L, Zhu G, Niu S M, Yu R M, Yang Q, Liu Y and Wang Z L 2013 *Nat. Photonics* **7** 752
[71] Dai J, Xu C X and Sun X W 2011 *Adv. Mater.* **23** 4115
[72] Bagnall D M, Chen Y F, Zhu Z, Yao T, Shen M Y and Goto T 1998 *Appl. Phys. Lett.* **73** 1038
[73] Klingshirn C 2007 *Phys. Status Solidi B* **244** 3027
[74] Hendry E, Koeberg M and Bonn M 2007 *Phys. Rev. B* **76** 045214
[75] Versteegh M A M, Vanmaekelbergh D and Dijkhuis J I 2012 *Phys. Rev. Lett.* **108** 157402
[76] Jamadi O, Reveret F, Disseix P, Medard F, Leymarie J, Moreau A, Solnyshkov D, Deparis C, Leroux M, Cambril E, Bouchoule S, Zuniga-Perez J and Malpuech G 2018 *Light Sci. Appl.* **7** 82
[77] Li F, Orosz L, Kamoun O, Bouchoule S, Brimont C, Disseix P, Guillet T, Lafosse X, Leroux M, Leymarie J, Mexis M, Mihailovic M, Patriarche G, Réveret F, Solnyshkov D, Zuniga-Perez J and Malpuech G 2013 *Phys. Rev. Lett.* **110** 196406
[78] Xie W, Dong H X, Zhang S F, Sun L X, Zhou W H, Ling Y J, Lu J, Shen X C and Chen Z H 2012 *Phys. Rev. Lett.* **108** 166401
[79] Feng J G, Wang J, Fieramosca A, Bao R Q, Zhao J X, Su R, Peng Y T, Liew T C H, Sanvitto D and Xiong Q H 2021 *Sci. Adv.* **7** eabj6627
[80] van Vugt L K, Rühle S, Ravindran P, Gerritsen H C, Kuipers L and Vanmaekelbergh D 2006 *Phys. Rev. Lett.* **97** 147401
[81] Sun L X, Chen Z H, Ren Q J, Yu K, Bai L H, Zhou W H, Xiong H, Zhu Z Q and Shen X C 2008 *Phys. Rev. Lett.* **100** 156403

[82] Dai J, Xu C X and Sun X W 2011 *Appl. Phys. Lett.* **98** 161110
[83] Lu J F, Zhu Q X, Zhu Z, Liu Y J, Wei M, Shi Z L and Xu C X 2016 *J. Mater. Chem. C* **4** 7718
[84] Dai J, Lu J F, Wang F, Guo J Y, Gu N and Xu C X 2015 *ACS Appl. Mater. Interfaces* **7** 12655
[85] Gargas D J, Gao H W, Wang H T and Yang P D 2011 *Nano Lett.* **11** 3792
[86] Chen R, Ye Q L, He T C, Ta V D, Ying Y J, Tay Y Y, Wu T and Sun H D 2013 *Nano Lett.* **13** 734
[87] Ding H Y, Zhao Z, Zhang G H, Wu Y K, Gao Z W, Li J W, Zhang K, Pan N and Wang X P 2012 *J. Phys. Chem. C* **116** 17294
[88] Wang R, Wang C F, Ma Y, Sun J L, Yan P G, Xu C X and Pan C F 2023 *Adv. Opt. Mater.* **11** 2203137
[89] Bergman D J and Stockman M I 2003 *Phys. Rev. Lett.* **90** 027402
[90] Oulton R F, Sorger V J, Zentgraf T, Ma R M, Gladden C, Dai L, Bartal G and Zhang X 2009 *Nature* **461** 629
[91] Noginov M A, Zhu G, Belgrave A M, Bakker R, Shalaev V M, Narimanov E E, Stout S, Herz E, Suteewong T and Wiesner U 2009 *Nature* **460** 1110
[92] Hill M T, Marell M, Leong E S P, Smalbrugge B, Zhu Y C, Sun M H, van Veldhoven P J, Geluk E J, Karouta F, Oei Y S, Nötzel R, Ning C Z and Smit M K 2009 *Opt. Express* **17** 11107
[93] Sidiropoulos T P H, Röder R, Geburt S, Hess O, Maier S A, Ronning C and Oulton R F 2014 *Nat. Phys.* **10** 870
[94] Chou Y H, Chou B T, Chiang C K, Lai Y Y, Yang C T, Li H, Lin T R, Lin C C, Kuo H C, Wang S C and Lu T C 2015 *ACS Nano* **9** 3978
[95] Lu J F, Jiang M M, Wei M, Xu C X, Wang S F, Zhu Z, Qin F F, Shi Z L and Pan C F 2017 *ACS Photonics* **4** 2419
[96] Liu Y, Jiang M M, He G H, Li S F, Zhang Z Z, Li B H, Zhao H F, Shan C X and Shen D Z 2017 *ACS Appl. Mater. Interfaces* **9** 40743
[97] Hwang D K, Kang S H, Lim J H, Yang E J, Oh J Y, Yang J H and Park S J 2005 *Appl. Phys. Lett.* **86** 222101
[98] Willander M, Nur O, Zhao Q X, Yang L L, Lorenz M, Cao B Q, Pérez J Z, Czekalla C, Zimmermann G, Grundmann M, Bakin A, Behrends A, Al-Suleiman M, El-Shaer A, Mofor A C, Postels B, Waag A, Boukos N, Travlos A, Kwack H S, Guinard J and Dang D L 2009 *Nanotechnology* **20** 332001
[99] Tang X B, Li G M and Zhou S M 2013 *Nano Lett.* **13** 5046
[100] Zhang X M, Lu M Y, Zhang Y, Chen L J and Wang Z L 2009 *Adv. Mater.* **21** 2767
[101] Lupan O, Pauporté T and Viana B 2010 *Adv. Mater.* **22** 3298
[102] Mao W Q, Jiang M M, Ji J L, Wan P, Zhou X B and Kan C X 2020 *Photonics Res.* **8** 175
[103] Wu Y T, Xu J, Jiang M M, Zhou X B, Wan P and Kan C X 2020 *CrystEngComm* **22** 2227
[104] Xu H Y, Liu Y C, Liu Y X, Xu C S, Shao C L and Mu R 2005 *Appl. Phys. B* **80** 871
[105] Ng A M C, Xi Y Y, Hsu Y F, Djurisic A B, Chan W K, Gwo S, Tam H L, Cheah K W, Fong P W K, Lui H F and Surya C 2009 *Nanotechnology* **20** 445201
[106] Chen C H, Chang S J, Chang S P, Li M J, Chen I C, Hsueh T J and Hsu C L 2009 *Appl. Phys. Lett.* **95** 223101
[107] Fu H K, Cheng C L, Wang C H, Lin T Y and Chen Y F 2009 *Adv. Funct. Mater.* **19** 3471
[108] Chen C P, Ke M Y, Liu C C, Chang Y J, Yang F H and Huang J J 2007 *Appl. Phys. Lett.* **91** 091107
[109] Liu Y D, Liang H W, Xia X C, Shen R S, Liu Y, Bian J M and Du G T 2012 *Appl. Phys. B* **109** 605
[110] Wang T, Wu H, Zheng H, Wang J B, Wang Z, Chen C, Xu Y and Liu C 2013 *Appl. Phys. Lett.* **102** 141912
[111] Yang L, Liu K, Xu H Y, Liu W Z, Ma J G, Zhang C, Liu C Y, Wang Z Q, Yang G C and Liu Y C 2017 *Adv. Opt. Mater.* **5** 1700493
[112] Jeong S and Kim H 2016 *Appl. Phys. Express* **9** 015501
[113] Chen A Q, Zhu H, Wu Y Y, Lou G L, Liang Y F, Li J Y, Chen Z Y, Ren Y H, Gui X C, Wang S P and Tang Z K 2017 *ACS Photonics* **4** 1286
[114] Cook T E, Jr, Fulton C C, Mecouch W J, Davis R F, Lucovsky G and Nemanich R J 2003 *J. Appl. Phys.* **94** 7155
[115] Chen Q, Yang M, Feng Y P, Chai J W, Zhang Z, Pan J S and Wang S J 2009 *Appl. Phys. Lett.* **95** 162104
[116] Huang H H, Fang G J, Li Y, Li S Z, Mo X M, Long H, Wang H N, Carroll D L and Zhao X Z 2012 *Appl. Phys. Lett.* **100** 233502
[117] Mo X M, Long H, Wang H N, Li S Z, Chen Z, Wan J W, Feng Y M, Liu Y P, Ouyang Y F and Fang G J 2014 *Appl. Phys. Lett.* **105** 063505
[118] Zhang L C, Li Q S, Shang L, Wang F F, Qu C and Zhao F Z 2013 *Opt. Express* **21** 16578
[119] Sun J W, Lu Y M, Liu Y C, Shen D Z, Zhang Z Z, Li B H, Zhang J Y, Yao B, Zhao D X and Fan X W 2008 *J. Phys. D* **41** 155103
[120] You J B, Zhang X W, Zhang S G, Wang J X, Yin Z G, Tan H R, Zhang W J, Chu P K, Cui B, Wowchak A M, Dabiran A M and Chow P P 2010 *Appl. Phys. Lett.* **96** 201102
[121] Sun L L, Li J T, Han J J, Liu M S, Meng M, Li B H and Jiang M M 2023 *Results Phys.* **54** 107065
[122] You D T, Xu C X, Qin F F, Zhu Z, Manohari A G, Xu W, Zhao J and Liu W 2018 *Sci. Bull.* **63** 38
[123] Ma Y, Wu M Y, Wan P, Jiang M M, Li Z X, Cui Q N, Shi Z L, Wang X X and Xu C X 2025 *J. Lightwave Technol.* **43** 4352
[124] Yang X, Shan C X, Ni P N, Jiang M M, Chen A Q, Zhu H, Zang J H, Lu Y J and Shen D Z 2018 *Nanoscale* **10** 9602
[125] Zhou X B, Jiang M M, Xu K, Liu M S, Sha S L, Cao S Y, Kan C X and Shi D N 2022 *Light Sci. Appl.* **11** 198
[126] Ma X Y, Pan J W, Chen P L, Li D S, Zhang H, Yang Y and Yang D R 2009 *Opt. Express* **17** 14426
[127] Zhu H, Shan C X, Zhang J Y, Zhang Z Z, Li B H, Zhao D X, Yao B, Shen D Z, Fan X W, Tang Z K, Hou X H and Choy K L 2010 *Adv. Mater.* **22** 1877
[128] Li Z X, Liu W, Wang R, Chen F, Chen J P, Zhu Y Z, Shi Z L and Xu C X 2022 *Nano Energy* **93** 106832
[129] Xu K, Wan P, Liu M S, Shi D N, Kan C X and Jiang M M 2024 *J. Mater. Chem. C* **12** 17818
[130] Xu K, Wan P, Liu M S, Tang K, Li L J, He T, Shi D N, Kan C X and Jiang M M 2024 *ACS Photonics* **11** 3276
[131] Lu J F, Liu W, Jiang M M, Zhou X B, Xu J, Liu Y, Kan C X, Shi D N and Xu C X 2021 *Appl. Phys. Lett.* **119** 131103
[132] Lu J F, Xu C X, Li F T, Yang Z, Peng Y Y, Li X Y, Que M L, Pan C F and Wang Z L 2018 *ACS Nano* **12** 11899
[133] Li Z X, Zhao J, Liu W, Zhu Y Z, Chen J P, Xu W X, Xia C S, Wang R, Cui Q N, Shi Z L and Xu C X 2022 *Adv. Opt. Mater.* **10** 2201080